Engineering Analysis with Boundary Elements 95 (2018) 93–104

Contents lists available at ScienceDirect

Engineering Analysis with Boundary Elements

journal homepage: www.elsevier.com/locate/enganabound

Trefftz methods with cracklets and their relation to BEM and MFS

Carlos J.S. Alves [a], Nuno F.M. Martins [b,*], Svilen S. Valtchev [a,c]

[a] CEMAT - IST, University of Lisbon, Av. Rovisco Pais 1, Lisboa 1049-001, Portugal
[b] Department of Mathematics, Faculdade de Ciências e Tecnologia, Univ. Nova de Lisboa, Quinta da Torre, Caparica 2829-516, Portugal
[c] ESTG - Polytechnic Institute of Leiria, Leiria 2411-901 Portugal

ARTICLE INFO

MSC:
65N38
65N80

Keywords:
Trefftz method
Cracklets
Boundary element method
Method of fundamental solutions

ABSTRACT

In this paper we consider Trefftz methods which are based on functions defined by single layer or double layer potentials, integrals of the fundamental solution, or their normal derivative, on cracks. These functions are called *cracklets*, and satisfy the partial differential equation, as long as the crack support is not placed inside the domain. A boundary element method (BEM) interpretation is to consider these cracks as elements of the original boundary, in a direct BEM approach, or elements of an artificial boundary, in an indirect BEM approach. In this paper we consider the cracklets just as basis functions in Trefftz methods, as the method of fundamental solutions (MFS). We focus on the 2D Laplace equation, and establish some comparisons and connections between these methods with cracklets and standard approaches like the BEM, indirect BEM, and the MFS. Namely, we propose the enrichment of the MFS basis with the cracklets. Several numerical simulations are presented to test the performance of the methods, in particular comparing the results with the MFS and the BEM.

1. Introduction

The solution of boundary value problems (BVP) for partial differential equations (PDEs) benefits from the fact that for homogeneous linear PDEs, it is possible to write them as a linear combination of basis functions that satisfy the PDE, reducing the BVP to the fitting of the boundary conditions. This is a general context of the Trefftz methods in its different variants (e.g. [20]), and it has the advantage that no meshing procedure is needed for the domain.

The Boundary Element Method (BEM) has also a long history of application (e.g. [12]) and it may be included in the class of Trefftz methods, as it relies on boundary potentials that are solutions of the PDE inside the domain. The indirect BEM (IBEM) is another Trefftz variant, where the boundary potentials are considered on some artificial boundary surrounding the original one. The use of an artificial boundary is also the context of application of another Trefftz method - the method of fundamental solutions (MFS), no longer with boundary potentials, but simply as the location of point sources, i.e. fundamental solutions centered on source points, that are located on some artificial boundary (e.g. [2,13,14]).

A connection between some of these approaches was already pointed out in [10], and in this paper we explore this known connection further, using the concept of *cracklets* (e.g. [1]). Since the single and double layer potentials are defined on a boundary, which is decomposed in multiple boundary elements, we consider the elements of the boundary themselves to be cracks (or screens), and the cracklets are therefore defined as single or double layers over the support of a crack. If the boundary elements are seen as the union of cracks, then the BEM formulation may be understood with the use of cracklets on the boundary, and the IBEM formulation with the use of cracklets on some artificial domain.

However since these cracklets are themselves solutions of the PDE, with an appropriate behavior at infinity, they might be understood as a Trefftz basis, and we propose that they may be used with no direct connection to a boundary (artificial or original). In Section 3.5 we prove a density theorem and its corollary that justifies the completeness of this set of basis functions.

As in the MFS, a good location for the support of the cracklets, is an issue of current research (cf. [2,8,22]), and we either considered a standard approach using boundary dilation, like in the IBEM, or used a MFS choice as proposed in [2], or even considered cracklets on the original boundary as in the BEM, as was proposed in [5] to tackle difficulties in the approximation of discontinuous functions. In particular, to avoid the Gibbs oscillations when approximating discontinuous boundary conditions (e.g. [16]).

Several different methods have been considered to avoid the singularities associated with the fundamental solutions and allowing direct collocation on the boundary, such as the boundary knot method [15], the regularized meshless method [23], the modified method of fundamental solutions [21], or the singular boundary method [11]. In Section 3.7 we emphasize that when the solution does not have an

* Corresponding author.
E-mail addresses: carlos.alves@math.tecnico.ulisboa.pt (C.J.S. Alves), nfm@fct.unl.pt (N.F.M. Martins), ssv@math.ist.utl.pt (S.S. Valtchev).

https://doi.org/10.1016/j.enganabound.2018.06.021
Received 30 May 2018; Accepted 23 June 2018
Available online 6 August 2018

analytic extension that goes beyond the analytic support of the approximation, the results will become worse. In fact it is known [7,18] that we can get exponential convergence of the MFS, as long as the solutions are entire, but the rate of convergence decreases fast, if the solutions do not extend analitically beyond the analytic support of the approximation, which is determined by the artificial boundary. In this sense the Trefftz method with cracklets proposed here is not attached to a specific artificial boundary as in an indirect boundary integral equation method. It inherits the ill conditioning of the inversion of compact operators (e.g. [19]), and these methods have been used to solve inverse problems, sharing the need of some regularization techniques (e.g. [4,17]).

The cracklets are here considered not only as a Trefftz method, but also as an enrichment technique for the MFS, for instance as proposed in [3,5,6], or to serve as a link between the MFS and the BEM. Recently, the method of angular basis functions (MABF) was proposed in [24,25] which considers double layer solutions, that are linked to angular measurements in the case of the Laplace equation. These functions are also considered in the fast implementation of BEM (e.g. [9]) and correspond to double layer cracklets.

In Section 2 we briefly recall the notions of layer potentials, and in Section 3 we consider the cracklet Trefftz method, as proposed for single and double layer potentials, but reduced to constant densities, and establish the main mathematical result that proves the completeness of the method. Finally in Section 4 we present numerical simulations that illustrate the performance of the different approaches.

2. Single and double layer potentials

This work will focus on harmonic boundary value problems, but it may be extended to problems such as

$$(P)\begin{cases} Du = 0, & \text{in } \Omega \\ Bu = g, & \text{on } \Gamma = \partial\Omega \end{cases} \tag{1}$$

where a fundamental solution Φ of the differential operator D is available.

In this paper, for simplicity, we assume $D = \Delta$ to be the 2D Laplace operator, with fundamental solution given by

$$\Phi(x) = \frac{1}{2\pi}\log||x||, \tag{2}$$

and when B is the identity operator, (P) is a Dirichlet boundary value problem, with unique solution $u \in H^1(\Omega)$, for a given $g \in H^{1/2}(\Gamma)$.

The corresponding single layer or double layer potentials (e.g. [19]) are respectively represented by $\mathcal{L}_\gamma$ and $\mathcal{M}_\gamma$,

$$\mathcal{L}_\gamma\alpha(x) = \int_\gamma \Phi(x-y)\alpha(y)ds_y \tag{3}$$

$$\mathcal{M}_\gamma\beta(x) = \int_\gamma \partial_{\boldsymbol{n}_y}\Phi(x-y)\beta(y)ds_y \tag{4}$$

where γ is a boundary that may coincide with Γ, $\alpha \in H^{-1/2}(\gamma)$ and $\beta \in H^{1/2}(\gamma)$ are unknown densities. Moreover, $\partial_{\boldsymbol{n}} = \nabla\cdot\boldsymbol{n}$ represents the normal derivative (we write $\partial_{\boldsymbol{n}_y}$ to be clear that the gradient is with respect to the y variable).

Remark 2.1. These layer potentials are defined for $x \notin \gamma$, and trace formulas may be obtained when $x \in \Omega \to x_\gamma \in \gamma$ (along the normal direction),

$$\mathcal{L}_\gamma\alpha(x) \to S_f\alpha(x_\gamma), \quad \mathcal{M}_f\beta(x) \to (\tau\mathcal{I} + \mathcal{K}_\gamma)\beta(x_\gamma) \tag{5}$$

where the expressions for S_f and $\mathcal{K}_\gamma$ are the same as for $\mathcal{L}_\gamma$ and $\mathcal{M}_\gamma$, respectively, but now with $x_\gamma \in \Gamma$, thus implying the definition of a (weakly) singular integral operator.

The parameter $\tau(x_\gamma) = \frac{1}{2}$ for all regular boundary points, but if x_γ is a corner point, then $\tau(x_\gamma) = \frac{\theta}{2\pi}$, where θ represents the internal angle (from 0 to 2π). Taking the trace from the exterior domain, with $x \notin \bar{\Omega}$, then τ has negative sign, corresponding to the external angle.

2.1. Integral equations

To find the unknown densities we consider the first kind integral equations when $x \in \Gamma$, and $\Gamma \neq \gamma$.

(i) Using the single layer potential, $\mathcal{L}_\gamma\alpha(x) = g(x)$, for $x \in \Gamma$, i.e.

$$\int_\gamma \Phi(x-y)\alpha(y)ds_y = g(x). \tag{6}$$

(ii) Using the double layer potential, $\mathcal{M}_\gamma\beta(x) = g(x)$, for $x \in \Gamma$, i.e.

$$\int_\gamma \partial_{\boldsymbol{n}_y}\Phi(x-y)\beta(y)ds_y = g(x). \tag{7}$$

Remark 2.2. When $\Gamma = \gamma$, we obtain

$$S\alpha(x) = g(x), \tag{8}$$

which is also a first kind integral equation on Γ, but a second kind integral equation is obtained for the double layer potential, since $(\tau\mathcal{I} + \mathcal{K})\beta(x) = g(x)$, which means

$$\tau(x)\beta(x) + \int_\Gamma \partial_{\boldsymbol{n}_y}\Phi(x-y)\beta(y)ds_y = g(x). \tag{9}$$

Remark 2.3. In the case of Neumann boundary conditions, the inner normal trace of the single and double layer potentials gives, when $x \in \Omega \to x_\gamma \in \gamma$ (along the normal direction),

$$\boldsymbol{n}(x_\gamma)\cdot\nabla\mathcal{L}_\gamma\alpha(x) \to (-\tau\mathcal{I} + \mathcal{K}'_\gamma)\alpha(x_\gamma) \tag{10}$$

$$\boldsymbol{n}(x_\gamma)\cdot\nabla\mathcal{M}_\gamma\beta(x) \to \mathcal{T}_\gamma\beta(x_\gamma) \tag{11}$$

with

$$\mathcal{K}'_\gamma\alpha(x_\gamma) = \int_\gamma \partial_{\boldsymbol{n}_x}\Phi(x_\gamma - y)\alpha(y)ds_y \quad \text{and}$$

$$\mathcal{T}_\gamma\beta(x_\gamma) = \int_\gamma \partial_{\boldsymbol{n}_x}\partial_{\boldsymbol{n}_y}\Phi(x_\gamma - y)\beta(y)ds_y.$$

The operator $\mathcal{T}_\gamma$ presents then a singular integration which is understood in the sense of the Cauchy principal value.

2.2. Direct and indirect boundary element approach

Consider the boundary element method in its two variants – the direct the and indirect approach.

(i) In the BEM, Eq. (8) or (9) are considered, taking $\gamma = \Gamma$.

(ii) In the IBEM, Eq. (6) or (7) are considered, with γ being an artificial boundary surrounding the original Γ. That is, we may take $\omega \supset \bar{\Omega}$ and $\gamma = \partial\omega$.

The integral equation (9) is of the second kind, it is better conditioned and usually preferred to the first kind integral equation (8).

The discretization of the integral operators on γ, equal or not to Γ, usually consists in splitting that boundary into boundary elements

$$\gamma = \gamma_1 \cup \cdots \cup \gamma_N \tag{12}$$

which may reproduce or approximate the full boundary. Thus,

$$\mathcal{M}\beta(x) = \sum_{n=1}^{N}\int_{\gamma_n} \partial_{\boldsymbol{n}_y}\Phi(x-y)\beta_n(y)ds_y \tag{13}$$

using local densities $\beta_n = \beta|_{\Gamma_n}$ and, for example, a trigonometric or a power series expansion, $\beta_n(s) = \beta_{n,0} + \beta_{n,1}s + \beta_{n,2}s^2 + \cdots$

In the simplest situation $\beta_n \cong \beta_{n,0}$ are constant terms, and the calculation resumes to the evaluation of

$$K_n(x) = \int_{\gamma_n} \partial_{\boldsymbol{n}_y}\Phi(x-y)ds_y \tag{14}$$

leading to the approximation

$$\mathcal{M}\beta(x) \approx \sum_{n=1}^{N}\beta_n K_n(x). \tag{15}$$

Using the boundary condition $(\tau I + \mathcal{K})\beta(x_k) = g(x_k)$ for points $x_k \in \Gamma$, we get the following linear system

$$\sum_{n=1}^{N} \big(\tau(x_k) I_n(x_k) + K_n(x_k)\big)\beta_n = g(x_k), \tag{16}$$

where $I_n(x_k) = \delta_{nk} = \begin{cases} 1, & \text{if } x_k \in \gamma_n, \\ 0, & \text{if } x_k \notin \gamma_n, \end{cases}$. In this case, the discretized solution is given by

$$u(x) = \mathcal{M}\beta(x) \approx \sum_{n=1}^{N} K_n(x)\beta_n \tag{17}$$

for $x \in \Omega$.

The difference between the direct and indirect approach consists in taking γ_n on Γ (direct BEM) or on the artificial boundary γ (indirect BEM), taking into account that in the indirect approach, the discretized boundary equation (16) is considered with $\tau \equiv 0$.

Advantages and disadvantages. A clear advantage of the BEM with the double layer approach is that it leads to a second kind integral equation, avoiding ill conditioning problems. But, on the other hand, the approximation on the boundary reflects the approximation being taken on β.

In the simplest situation, while considering an approximation by piecewise constant densities, the approximation on the boundary will be affected by the discontinuous approximation of the density, and this is not suited for more regular boundary conditions, as a better approximation requires more basis functions and a larger system.

On the other hand, the indirect approach may lead to an analytic approximation of the boundary condition, but this might be inconvenient for discontinuous boundary conditions. Moreover it leads to ill conditioned systems, and the major problem is that it defines an extension of the solution outside Ω.

This is the same problem that may occur with the MFS, while taking an artificial boundary $\gamma = \partial\omega$. Thus, we will proceed in the same direction, proposing a Trefftz method with cracklets placed outside Ω, as is done with point sources in the MFS.

3. A Trefftz method with cracklet functions

We will consider as basis functions for the Trefftz method, the *cracklet functions* as they will be defined entirely by the crack location γ_n outside Ω. In the limit, if we consider these cracks to be located on the boundary Γ, we get the same approach as in the boundary element method.

3.1. Double layer cracklets

We start with the double layer cracklets, because their expression is simpler. In fact, we define the cracklets K by

$$K(\gamma_n)(x) = \int_{\gamma_n} \partial_{\boldsymbol{n}_y} \Phi(x-y) ds_y, \tag{18}$$

and this calculation may be reduced to a reference linear crack $\gamma_\varepsilon = [0,\varepsilon]\times\{0\}$, by a rigid transformation $\gamma_n = a_n + Q\gamma_\varepsilon$, when γ_n is a linear crack, with Q being a rotation matrix, and $\varepsilon = |\gamma_n|$ being the length of the cracklet.

For the Laplace equation in 2D,

$$K(\gamma_\varepsilon)(x) = \frac{1}{2\pi}\left(\arctan\left(\frac{\varepsilon - x_1}{x_2}\right) + \arctan\left(\frac{x_1}{x_2}\right)\right) \tag{19}$$

Remark 3.1. Considering the complex Argand plane, K may be written as (e.g. [9])

$$K(\gamma)(z) = \frac{1}{2\pi}(\arg(b-z) - \arg(a-z)), \tag{20}$$

for a line crack $\gamma = [a,b]$, where $a, b, z \in \mathbb{C}$.

In Fig. 1 we present the cracklet function $u = K(\gamma_\varepsilon)$ with $\varepsilon = 1$, which presents a discontinuity with a jump $[u] = u^- - u^+ = 1$. On the other hand, the normal derivative is continuous across the crack, that is $[\partial_n u] = 0$.

3.2. Single layer cracklets

In this case, we define the cracklets S by

$$S(\gamma_n)(x) = \int_{\gamma_n} \Phi(x-y) ds_y, \tag{21}$$

and this calculation may again be reduced to a reference linear crack $\gamma_\varepsilon = [0,\varepsilon]\times\{0\}$, by the same rigid transformation $\gamma_n = a_n + Q\gamma_\varepsilon$.

For the Laplace equation in 2D,

$$S(\gamma_\varepsilon)(x) = \frac{\varepsilon}{2\pi} - x_2 K(\gamma_\varepsilon)(x) + \frac{x_1 - \varepsilon}{2\pi}\log(||x - (\varepsilon,0)||) - \frac{x_1}{2\pi}\log(||x||). \tag{22}$$

In Fig. 1 we present the cracklet function $v = S(\gamma_\varepsilon)$ with $\varepsilon = 1$. In this case the function is continuous across the crack $[v] = 0$, and if fact when $x \in \gamma_\varepsilon$

$$v(x) = S(\gamma_\varepsilon)(x) = \frac{\varepsilon}{2\pi} + \frac{x_1 - \varepsilon}{2\pi}\log|x_1 - \varepsilon| - \frac{x_1}{2\pi}\log|x_1|$$

and $v(x) = \frac{\varepsilon}{2\pi}$ on both tips of the crack. A jump appears only on the normal derivative through γ_ε.

Remark 3.2. We are only considering here the simplest cracklets, with constant density, but it is clear that we could also consider more complex cracklets (cf. [5]) using, for instance, polynomial densities up to degree p, with

$$S_p(\gamma_n)(x) = \int_{\gamma_n} \Phi(x-y)\, y^p\, ds_y \quad \text{and} \quad K_p(\gamma_n)(x) = \int_{\gamma_n} \partial_{\boldsymbol{n}_y}\Phi(x-y)\, y^p\, ds_y. \tag{23}$$

3.3. Trefftz methods with cracklets

We do not require that the union of the cracks $\gamma_1 \cup \cdots \cup \gamma_N$ forms a closed boundary.

Taking γ_n outside Ω, each cracklet $K(\gamma_n)$ or $S(\gamma_n)$ is a solution of the PDE in Ω. We do not exclude that $\gamma_n \subset \Gamma$, and in that case, the cracklet may be understood as a boundary element.

Therefore a linear combination of these particular solutions gives also a solution of the PDE.

(i) Using cracklets K, the approximation will be

$$u_N(x) = \sum_{n=1}^{N} \beta_n K(\gamma_n)(x), \tag{24}$$

calculating β_n from the system

$$\big[K(\gamma_n)(x_m^-)\big]\big[\beta_n\big] = \big[g(x_m)\big], \tag{25}$$

where $x_m \in \Gamma$, are collocation points.

Remark 3.3. It is important to notice that we write $x_m^- = x_m - \varepsilon \boldsymbol{n}(x_m)$, with $\varepsilon \to 0^+$, to include the case when $\gamma_n \subset \Gamma$. Taking into account the trace formula (9), system (25) resumes to

$$\left[\frac{1}{2}\delta_{nm} + K(\gamma_n)(x_m)\right]\big[\beta_n\big] = \big[g(x_m)\big]. \tag{26}$$

(ii) Using cracklets S, it is similar, as the approximation will be

$$v_N(x) = \sum_{n=1}^{N} \alpha_n S(\gamma_n)(x), \tag{27}$$

calculating α_n from the system

$$\big[S(\gamma_n)(x_m)\big]\big[\alpha_n\big] = \big[g(x_m)\big]. \tag{28}$$

Example 3.4. In the simplest situation, we may consider the domain to be a square $\Omega = (-1,1)^2$, and double layer cracklets on the four edges of the square, $\partial\Omega = \gamma_1 \cup \gamma_2 \cup \gamma_3 \cup \gamma_4$.

In this example we are using a direct BEM method, and we may use the middle points on each edge to collocate and get the system. Using the complex notation we get

$$K(\gamma_n)(z) = \frac{1}{2\pi}(\arg(q_{n+1} - z) - \arg(q_n - z)),$$

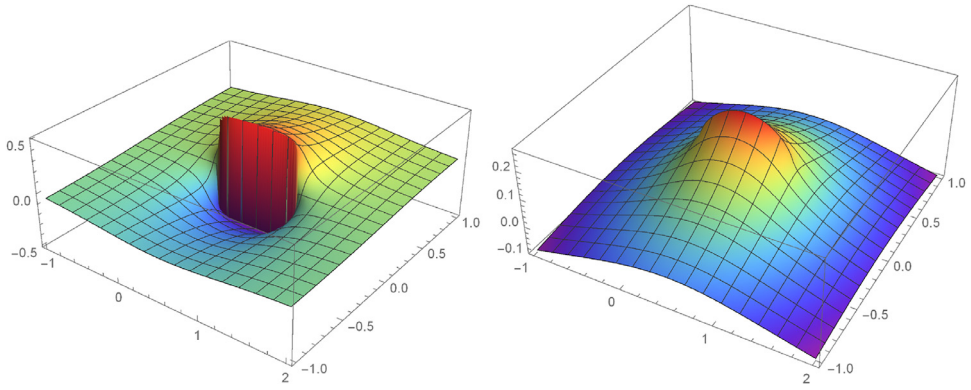

Fig. 1. Cracklets for the double layer potential ($K(\gamma_\epsilon)$ on the left picture), and for the single layer potential ($S(\gamma_\epsilon)$ on the right picture), with $\epsilon = 1$.

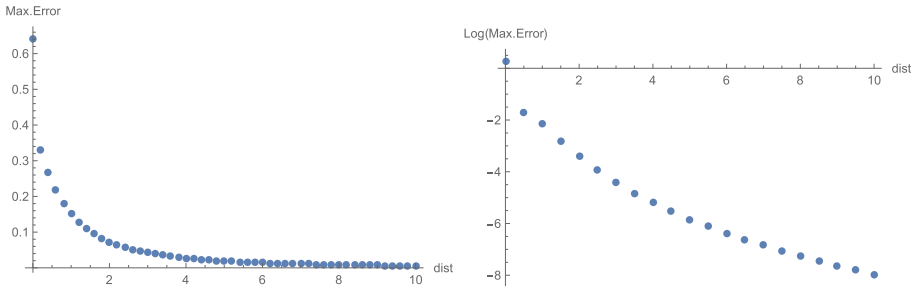

Fig. 2. Example 1. On the left, approximation of the maximum error with $N = 4$ cracklets for $g(z) = z$, decreasing with larger distance to the boundary. On the right, the same experiment with $N = 32$, for $g(z) = z^p$, taking the average of the maximum errors for $p = 0, \dots, 8$, here presented in log_{10} scale.

using $q_1, \dots, q_4$ as the complex coordinates for the vertices, and assuming $q_5 = q_1$. This leads to the matrix

$$M_{mn} = K(\gamma_n)(z_m) = \frac{1}{2\pi}\big(\arg\left(q_{n+1} - z_m\right) - \arg\left(q_n - z_m\right)\big).$$

Taking as collocation points $z_m = \frac{1}{2}(q_m + q_{m+1})$, the system resumes to be

$$\left(\frac{1}{2}\boldsymbol{I} + \begin{bmatrix} 0 & c & t & c \\ c & 0 & c & t \\ t & c & 0 & c \\ c & t & c & 0 \end{bmatrix}\right)\begin{bmatrix}\beta_1\\ \beta_2\\ \beta_3\\ \beta_4\end{bmatrix} = \begin{bmatrix} \frac{1}{2} & c & t & c \\ c & \frac{1}{2} & c & t \\ t & c & \frac{1}{2} & c \\ c & t & c & \frac{1}{2} \end{bmatrix}\begin{bmatrix}\beta_1\\ \beta_2\\ \beta_3\\ \beta_4\end{bmatrix} = \begin{bmatrix}g_1\\ g_2\\ g_3\\ g_4\end{bmatrix}$$

where $c = \frac{1-2t}{4}$, $t = \frac{1}{2} - \frac{\arctan(2)}{\pi} = 0.147584..$, and $g_m = g(z_m)$.

When $g(z) = 1$, and since $2c + t = \frac{1}{2}$, the solution is $\beta_1 = \cdots = \beta_4 = 1$, therefore

$$u(z) = \sum_{n=1}^{4} K(\gamma_n)(z) = \sum_{n=1}^{4} \frac{1}{2\pi}(\arg(q_{n+1} - z) - \arg(q_n - z))$$
$$= \frac{1}{2\pi}\big(\arg(q_5 - z) - \arg(q_1 - z)\big).$$

Since $q_5 = q_1$, for points z outside the square, the argument does not jump and $u(z) = 0$, but for points z inside the square the argument rotates by 2π, and $u(z) = 1$, giving the exact solution inside the square. In fact, while using the argument function or arctangent, some attention must be given to the implementation.

A similar result can be obtained for a larger square $\hat{\Omega} = (-a, a)^2$ with $a > 1$, giving the same exact solution for the indirect BEM, although for a different matrix with diagonal entries $M_{jj} = \frac{1}{\pi}\arctan(\frac{a}{a-1})$.

However, for $g(z) = z$ it is clear that the approximation does no longer yield an exact result. Moreover, the best result is not given with the cracklets on the original boundary. The error converges to zero as the distance of the artificial boundary goes from zero to infinity. When the distance is zero, and the boundaries coincide, the maximum error is 0.65, and when the distance is 10 it is only 5.81×10^{-3} (see Fig. 2, on the left). Moreover, using $N = 8$ cracklets (two on each edge), the maximum error decreases from 0.357.. to 1.84×10^{-5}, and with $N = 16$ the maximum error decreases from 0.21 to 8.51×10^{-10}. Even if we consider monomials $g(z) = z^p$ up to degree $p = 8$ (or more), the results are extremely good with $N = 32$ cracklets at a distance $d = 10$, giving an average maximum error of 10^{-8} (see Fig. 2, right).

Thus, we may conclude that a few cracklets allow to approximate harmonic polynomials up to a considerable degree, with extremely small errors.

In fact, since we observe that $||z^p - u_{32,p}(z)||_\infty \leq 10^{-8}$, we have for polynomials $P_8(z) = \sum_{p=0}^{8} a_p z^p$ that $u_{32}(z) = \sum_{p=0}^{8} a_p u_{32,p}(z)$ satisfies

$$||P_8(z) - u_{32}(z)||_\infty \leq \sum_{p=0}^{8} |a_p|\ ||z^p - u_{32,p}(z)||_\infty \leq 10^{-8} \sum_{p=0}^{8} |a_p|.$$

Remark 3.5. Since any analytic function in $\mathbb{C}$ has a power series expansion, in Laurent series, we can capture a considerable number of functions with good precision, using just 32 cracklets. This is not only true for the square, but also for any other shape inside the square.

Example 3.6. The excellent results obtained for traces of harmonic polynomials, do not occur for non harmonic polynomials. Consider polynomials of the form $g(z) = Re(z)^p$ which do not satisfy the Laplace equation, for $p \geq 2$, and vary N from 32 to 128 elements. The smallest maximum error is achieved at a variable distance, which is about the length of the distance between the collocation points (in this case, $d = 8/N$). These results are shown in Fig. 3, left (due to some numerical ill conditioning, the linear system was solved in the least squares sense).

We must note that when the cracklets are close to the boundary, the system matrix presents diagonal elements that are close to 1, and the other entries are comparatively very small, but not small enough to give a diagonally dominant matrix.

In Fig 3, right, we plot a similar result for boundary functions $g(z) = |z|^p$, which also do not satisfy the Laplace equation. We took the distance to be $d = 8/N$, and considered $N = 2^m$ cracklets, taking the

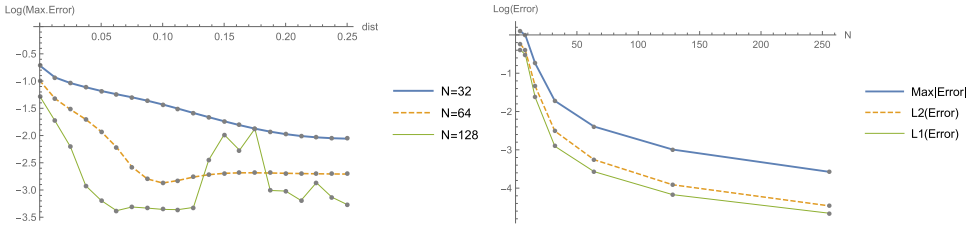

Fig. 3. Example 2. On the left, approximation maximum error for $g(z) = Re(z)^p$, with $N = 32$, 64 and 128 cracklets decreasing near the boundary. On the right, a similar experiment with $g(z) = |z|^p$, taking the average errors for $p = 1, \dots, 4$, here presented in log_{10} scale for three different norms.

average errors up to $p = 4$. In this case we considered not only the maximum norm, but also a discrete ℓ^2 norm, using P test points $z_1, \dots, z_P \in \partial\Omega$ (with $P \gg N$). This norm is given by

$$||g - u_N||^2_{\ell^2} = \frac{1}{P}\sum_{p=1}^{P} |g(z_p) - u_N(z_p)|^2, \tag{29}$$

and this may be seen to approximate the $L^2(\Gamma)$ norm, because

$$\begin{aligned} ||g - u_N||^2_{L^2(\Gamma)} &= \int_\Gamma |g(z) - u_N(z)|^2 dz \\ &\approx \sum_{p=1}^{P} \int_{[z_p, z_{p+1}]} |g(z) - u_N(z)|^2 dz \\ &\approx \sum_{p=1}^{P} |g(z_p) - u_N(z_p)|^2 |z_{p+1} - z_p| \\ &\approx \frac{|\Gamma|}{P}\sum_{p=1}^{P} |g(z_p) - u_N(z_p)|^2 \end{aligned}$$

assuming that the points are almost equally spaced and $|z_{p+1} - z_p| \approx \frac{|\Gamma|}{P}$. The only difference is that we neglect the length of the boundary $|\Gamma|$, like we do in the ℓ^1 average error

$$||g - u_N||_{\ell^1} = \frac{1}{P}\sum_{p=1}^{P} |g(z_p) - u_N(z_p)|, \tag{30}$$

that approximates $\frac{1}{|\Gamma|}||g - u_N||_{L^1(\Gamma)}$, the averaged $L^1(\Gamma)$ norm.

3.4. Connection with the MFS

An approximation with the method of fundamental solutions can be considered as a combination

$$v_N(x) = \sum_{k=1}^{N} a_k \Phi(x - y_k) + \sum_{k=1}^{N} \boldsymbol{b}_k \cdot \nabla\Phi(x - y_k), \tag{31}$$

using only monopolar sources (with $\boldsymbol{b}_k \equiv \boldsymbol{0}$, which is the classical case) or also using dipolar sources, that might follow a prescribed direction $\boldsymbol{b}_k = \boldsymbol{n}(y_k)b_k$, corresponding to a discretization of the double layer potential on the artificial boundary. The connection of the MFS with the boundary layers is well known, and we provide here some error estimates considering cracklets.

Taking a cracklet defined by the single layer potential on a small γ, with a middle point y_m, the mid-point integration rule gives for x not close to the boundary

$$S(\gamma)(x) = \int_\gamma \Phi(x - y) ds_y = \Phi(x - y_m)|\gamma| + O(|\gamma|^3) \tag{32}$$

with $|\gamma|$ being the length of the cracklet support.

Thus, this small cracklet is expected to have a similar effect as considering a point source at y_m as a pole. A similar reasoning occurs for the double layer potential,

$$K(\gamma)(x) = \int_\gamma \partial_{\boldsymbol{n}_y}\Phi(x - y) ds_y \approx \boldsymbol{n}(y_m) \cdot \nabla\Phi(x - y_m)|\gamma| \tag{33}$$

relating it to the dipole centered in y_m with direction given by the normal.

Therefore, the use of very small single layer cracklets, at some distance from the boundary, will have a similar effect as the use of the standard MFS (and the use of small double layer cracklets will be similar to a dipole MFS). We resume this in the following theorem (that may also be deduced for the double layer cracklets).

Theorem 3.7. *Consider line cracks such that $|\gamma_n| \le \varepsilon$ and dist$(\Omega, \gamma_n) > 0$. Then an approximation using cracklets S, given by*

$$u_N(x) = \sum_{n=1}^{N} \alpha_n S(\gamma_n)(x) \tag{34}$$

with $|\alpha_n| \le ||\boldsymbol{\alpha}||_\infty$, can be reproduced by a standard MFS approximation

$$v_N(x) = \sum_{k=1}^{N} \alpha_n |\gamma_n| \Phi(x - y_n) \tag{35}$$

where y_n is the middle point of γ_n, with the following error estimate for $x \in \bar{\Omega}$,

$$|u_N(x) - v_N(x)| \le \frac{N||\boldsymbol{\alpha}||_\infty \varepsilon^3}{48\pi dist(\Omega, \gamma)^2}. \tag{36}$$

Proof. It is an immediate consequence of (32), more precisely for $x \in \bar{\Omega}$

$$\left| \int_{\gamma_n} \Phi(x - y) ds_y - \Phi(x - y_n)|\gamma_n| \right| \le \frac{|\gamma_n|^3}{48\pi dist(\Omega, \gamma_n)^2}$$

which is a consequence of the middle point integration error estimate, since $|\partial^2_{ij}\Phi(x)| \le \frac{1}{2\pi||x||^2}$. Thus,

$$|u_N(x) - v_N(x)| \le \sum_{n=1}^{N} |\alpha_n| \left| S(\gamma_n)(x) - |\gamma_n|\Phi(x - y_n) \right| \le \sum_{n=1}^{N} \frac{|\alpha_n||\gamma_n|^3}{48\pi dist(\Omega, \gamma_n)^2}.$$

□

3.5. Completeness of the cracklets

Here we present a theorem for the completeness of external cracklets in $L^2(\Gamma)$.

Theorem 3.8. *Let $\omega \supset \bar{\Omega}$, and consider the spaces of cracklets on $\gamma = \partial\omega$, defined by*

$$\mathcal{G}_S = \text{span}\{ S(\gamma_{[y,\varepsilon]}) : \ y \in \gamma, \varepsilon > 0 \} \cup \{1\}, \tag{37}$$

$$\mathcal{G}_K = \text{span}\{ K(\gamma_{[y,\varepsilon]}) : \ y \in \gamma, \varepsilon > 0 \}, \tag{38}$$

where $\gamma_{[y,\,\varepsilon]}$ is a part of the boundary, connecting $y \in \gamma$ to $\tilde{y} \in \gamma$ such that $||y - \tilde{y}|| = \varepsilon$. Then $\mathcal{G}_S$ and $\mathcal{G}_K$ are dense in $L^2(\Gamma)$.

Proof. We prove the result for $\mathcal{G}_S$ (the proof for $\mathcal{G}_K$ is similar).

Consider any discrete number of points $y_1, \dots, y_N \in \gamma$, such that when $N \to \infty$, this set of points is dense in γ. We assume that $||y_{k+1} - y_k|| = \varepsilon > 0$, such that $y_{N+1} = y_1$.

Given any function $\psi \in L^2(\Gamma)$, we want to prove that the orthogonality of the cracklets implies ψ to be null. That is, if

$$\left\langle S(\gamma_{[y,\varepsilon]}),\psi\right\rangle_{L^2(\Gamma)} = \int_\Gamma S(\gamma_{[y,\varepsilon]})(x)\psi(x)dx = \int_\Gamma\int_{\gamma_{[y,\varepsilon]}} \Phi(x-s)ds\,\psi(x)dx = 0$$

then $\psi\equiv 0$. Using this equality for each y_n we define any linear combination of cracklets

$$v(x) = \sum_{n=1}^{N}\alpha_n S(\gamma_{[y_n,\epsilon]})(x) = \int_\gamma \alpha(s)\Phi(x-s)ds$$

while considering $\alpha(s)=\alpha_n$, when $s\in\gamma_{[y_n,\epsilon]}$, and we have

$$\langle v,\psi\rangle_{L^2(\Gamma)} = \sum_{n=1}^{N}\alpha_n\left\langle S(\gamma_{[y,\epsilon]}),\psi\right\rangle_{L^2(\Gamma)} = \int_\Gamma\int_\gamma \alpha(s)\Phi(x-s)ds\,\psi(x)dx = 0.$$

This means that for any piecewise constant density α, we get

$$\int_\gamma \alpha(s)\int_\Gamma \Phi(x-s)\psi(x)dx\,ds = 0.$$

As this is true for any $\varepsilon>0$, from the previous weak equality, we conclude the strong equality

$$u(s) = \int_\Gamma \Phi(x-s)\psi(x)dx = 0,$$

when $s\in\gamma$.

Since u satisfies the null exterior Dirichlet problem in $\omega^c=\mathbb{R}^2\backslash\bar{\omega}$ and it is ortogonal to constants, this implies $u\equiv 0$ in $\mathbb{R}^2\backslash\bar{\Omega}$, by analytic extension. As u is defined by a continuous single layer potential on Γ, then $[u]=0$, and $u^-=u^+=0$. The uniqueness of the interior Dirichlet problem also implies that $u\equiv 0$ in Ω, and this forces $\psi\equiv 0$. □

Corollary 3.9. *In Theorem 3.8 we may consider any set $\gamma\subset\Omega^c$ as long as there is a boundary $\gamma^\star\subseteq\gamma$, with $\gamma^\star=\partial\omega^\star$ and $\omega^\star\supset\bar{\Omega}$.*

Proof. This is a consequence of the proof of Theorem 3.8, since $u(s)=0$ with $s\in\gamma$ implies, in particular, that $u(s)=0$ with $s\in\gamma^\star$, and the other steps remain true taking $\gamma^\star$ instead of γ. □

Remark 3.10. Theorem 3.8 does not specify which kind of artificial ω to consider, and we may assume that it is a polygon, such that each crack $\gamma_{[y_n,\epsilon]}$ is a straight segment. Therefore, due to the corollary, we may consider intersecting crack supports that in the limit contain an exterior artificial boundary.

Remark 3.11. As previously mentioned when $\gamma\subset\Omega^c$, the inversion of S_γ or $\mathcal{K}_\gamma$ leads to ill-posed problems, because they imply the inversion of compact operators. Therefore we can not have $S_\gamma\alpha=g$ or $\mathcal{K}_\gamma\beta=g$ with $||\alpha||$, $||\beta||<\infty$. On the other hand, this theorem implies that we may find a sequence of α_n or of β_n such that $||S_\gamma\alpha_n-g||\to 0$ or $||\mathcal{K}_\gamma\beta_n-g||\to 0$. The main problem is that, in that case, $||\alpha_n||\to\infty$ and $||\beta_n||\to\infty$.

Thus, like in the MFS, we expect that the coefficients in the solution of the linear system will tend to infinity, unless some regularization technique (like Tikhonov regularization) is used. The ill conditioning problems of the MFS will appear also using cracklets, or using a similar indirect BEM.

3.6. Neumann boundary conditions

In the case of Neumann boundary conditions, the procedure is basically the same.

Moreover, using the single layer potential cracklets, the gradient of the reference cracklet is given by the vector

$$\nabla S(\gamma_\varepsilon)(x) = \begin{bmatrix}\Phi(x-(\varepsilon,0))-\Phi(x)\\ -K(\gamma_\varepsilon)(x)\end{bmatrix}. \tag{39}$$

In the reference crack we may consider the normal vector to be (0,1), giving exactly

$$\partial_{\boldsymbol{n}_x} S(\gamma_\varepsilon) = -K(\gamma_\varepsilon),$$

and this means that we may use the double layer cracklets directly for the Neumann problem, as long as we understand that the density being recovered in the system is α, to be used in the single layer representation (and not β which was used for the double layer representation).

This results from the duality between the expression for the trace of the double layer (9), and the normal trace of the single layer given in (10), and is well known in the BEM. It does not change much if we take the normal derivative on a boundary Γ which is different from γ, as long as the normal vector is the same. For instance, considering line cracklets, parallel to a polygonal boundary.

In any case, with the expression of the gradient being available, for any cracklet (by rigid transformation), we just have to solve the linear system

$$\left[\boldsymbol{n}(x_m)\cdot\nabla S(\gamma_n)(x_m^-)\right]\left[\alpha_n\right] = \left[g_{\mathbf{n}}(x_m)\right] \tag{40}$$

(here $g_{\mathbf{n}}(x_m)$ represents the Neumann data on $x_m\in\gamma$), and the solution will be given by the discrete single layer representation (27).

Another possibility is to consider the gradient of the double layer representation, giving

$$\nabla K(\gamma_\varepsilon)(x) = \frac{-\varepsilon}{2\pi||x-(\varepsilon,0)||^2||x||^2}\begin{bmatrix}(\varepsilon-2x_1)x_2\\ (\varepsilon-x_1)x_1+x_2^2\end{bmatrix}$$

with singularities on the tips, and this is associated with the singular operator $\mathcal{T}_\gamma$ as defined in (11), when Γ and γ coincide.

3.7. Analytic support

The use of cracklets as basis functions to solve boundary value problems can be seen, in the limiting case as a BEM, when the union of γ_n coincides with Γ, or the indirect BEM, when that union γ is a boundary that surrounds Γ.

With this flexibility it can be used to either capture the advantages of one or the other.

Moreover, since the cracklets are used as basis functions, we do not require them to replicate a full boundary, we can place some cracklets near the boundary (for instance, when discontinuities are present or expected), and some other cracklets away from the boundary.

The main goal is just to diminish the boundary error, and approximate g as well as possible, since all the functions satisfy the PDE.

Unlike the BEM, we do not propose to increase the polynomial degree of the density approximation, using functions S_p or K_p (as it was mentioned in Remark 3.2), with higher p, unless this is strictly necessary – and in that case it is clear that the standard BEM will perform better.

We propose to place the cracklets at a reasonable distance from the original boundary, as their trace leads to analytical functions on the boundary. The compromise is that the system will become more ill conditioned, as occurs in the MFS.

In fact, the use of cracklets may be combined with the MFS, taking the advantages of one and the other. The use of cracklets may be seen as an enrichment of the MFS basis, as it was already done in [5] to solve boundary value problems with discontinuities on the Dirichlet data.

The best performance of a method is related to the type of boundary functions being tested, and if a method suits better to some of them, it may fail considerably for others. The main difficulties for the Trefftz methods appear in approximating solutions with smaller analytical support than the basis, and in increasing the ill conditioning of the linear systems to be solved.

Remark 3.12. Consider a Trefftz basis $\phi_1,\dots,\phi_n,\dots$ that has analytical support in a set $\hat{\Omega}$ and a solution u with analytic support in $\tilde{\Omega}\supseteq\Omega$. If $\tilde{\Omega}\subset\hat{\Omega}$ then it is impossible to write u as a linear combination of ϕ_n. This does not imply that it is not possible to approximate u with a linear combination of ϕ_n, in appropriate norms. In fact, assume that $v=\sum_n\alpha_n\phi_n$ satisfies $v\equiv u$ in $\Omega\subseteq\tilde{\Omega}$. As the analytical support of v is $\hat{\Omega}$, by the analytical continuation theorem, it is possible to extend analytically v from $\tilde{\Omega}$ to $\hat{\Omega}$. However this is not true for u as its analytical support is reduced to $\tilde{\Omega}$ and these sets are different.

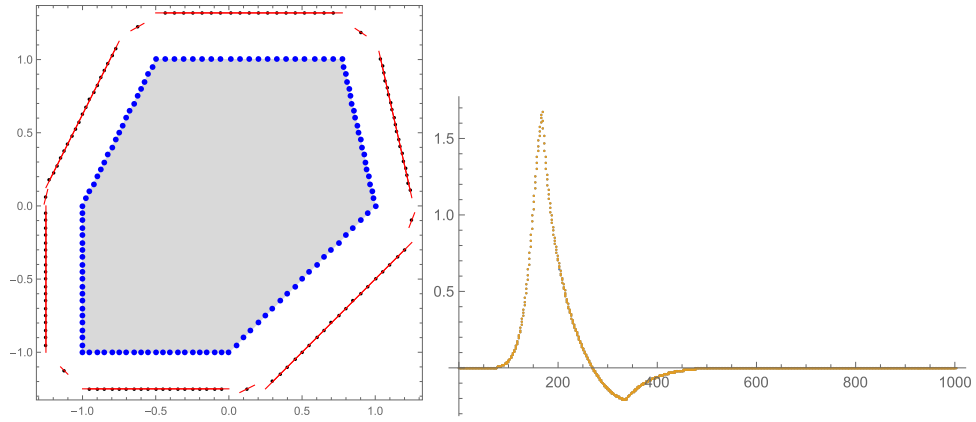

Fig. 4. Simulation 1. On the left, the domain of approximation with the collocation points (120 blue points) on the boundary $\partial\Omega_1$, and the cracklets (in red) using the procedure defined in (41). On the right, the values of the function g_a along 1002 test points on the polygonal boundary. (For interpretation of the references to color in this figure legend, the reader is referred to the web version of this article.)

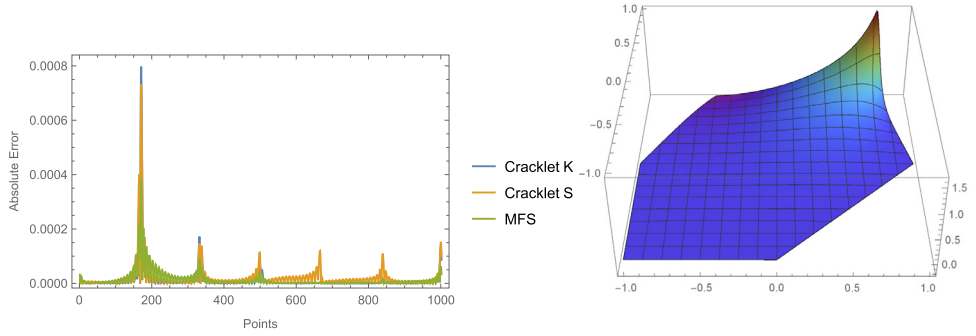

Fig. 5. Simulation 1. On the left, absolute errors for 3 methods – using Cracklets K or S, and using the MFS, with the boundary function g_a. On the right, plot of the solution in the polygonal domain.

In the case of the MFS, it is known that the method performs better when the point sources are placed far from the boundary [18], if the solution extends as an analytic function to infinity, meaning that $\tilde{\Omega} = \mathbb{R}^2$. The same performance was seen here with cracklets taken far away from the boundary. In these situations there is no problem as $\hat{\Omega} \subset \mathbb{R}^2$. But in these situations also polynomials, or other analytic functions, satisfying the PDE, could be used in a Trefftz method.

However, if the solution does not extend analytically outside the domain, i.e.$\tilde{\Omega} = \Omega$ the best possibility would be to consider the BEM, even if the approximation on the boundary is not so great.

Frequently there is an analytic extension of the solution outside Ω but it may be constrained in some parts of the boundary, for instance, corners, or discontinuities on the boundary condition. In those situations, the best strategy is to combine methods. On the part of the boundary where no analytic extension is expected, we may use cracklets very close to the boundary, like in the BEM, and on the part of the boundary where no problems are expected, the cracklets may be placed away from the boundary, like in the MFS.

4. Numerical simulations

We consider some experiments that show the performance of the proposed methods, for non trivial domains, and compare them with the MFS and the BEM.

There are several known factors that may change the quality of the approximation, concerning the position of the point sources in the MFS, and in this case the position, orientation and length of the cracklets. We will focus on some specific approximations that worked well, but better results may be obtained for each of the methods, depending on the geometry of the domain and on the boundary functions.

Sinc Trefftz methods yield in general ill conditioned systems, the linear systems were solved in the least squares sense (a Tikhonov regularization factor was not needed in these examples). This would not be needed for cracklets very close to the boundary, as this would lead a to well conditioned system, especially for cracklets K, nevertheless, as this will not change the $N \times N$ system solution, as we are dealing with square matrices. The matrices are rectangular only for the MFS which is considered with $2N$ collocation points.

4.1. Simulation 1 (polygonal domain)

Consider a polygonal domain Ω_1 defined by the six vertices with complex coordinates $\{1, \frac{3}{4}+i, i-\frac{1}{2}, -1, -1-i, -i\}$.

We divided each segment in the same number of points, that acted as collocation points, $x_1, \ldots, x_M$. From these set points we defined the cracklets, as segments $]y_m^-, y_m^+[$ with tips given by

$$y_m = x_m + \delta_m \boldsymbol{t}_m^{\perp} \quad \text{and} \quad y_m^{\pm} = y_m \pm \theta_m \boldsymbol{t}_m, \tag{41}$$

where $\boldsymbol{t}_m = \frac{1}{2}(x_{m+1} - x_{m-1})$ and $\boldsymbol{t}_m^{\perp}$ is orthogonal to t_m, pointing in the normal direction (or its average). The choice of y_m has already been used for the MFS (e.g. [2]).

The parameter δ_m reflects the distance to the boundary with respect to the distance between points, and the parameter θ_m reflects half the length of the crack with a middle point given by y_m. Keeping the size of the crack with respect to the distance between collocation points, this means $\theta_m = 1$, which was the best choice that we considered.

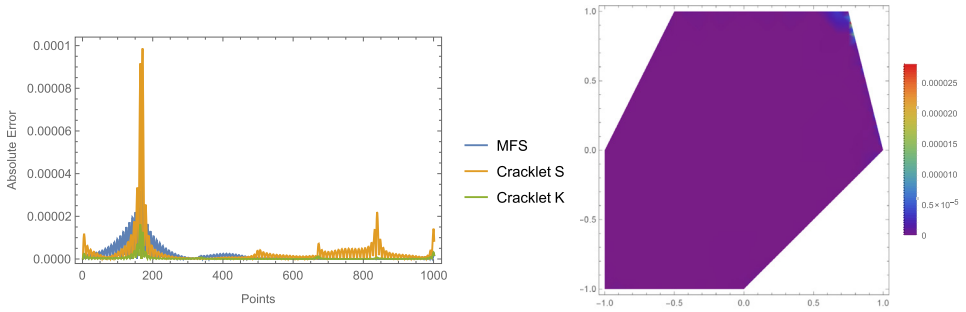

Fig. 6. Simulation 1. On the left, absolute error plots for the three methods, considering the boundary function g_b. On the right, density plot of the absolute error in the domain for the Cracklet K approximation.

Table 1
Errors in different norms for the different methods, considered for simulation 1 with g_a.

	$\|\|g_a - u_{120}\|\|_\infty$	$\|\|g_a - u_{120}\|\|_{\ell^2}$	$\|\|g_a - u_{120}\|\|_{\ell^1}$
BEM S	0.078	5.8×10^{-3}	1.4×10^{-3}
BEM K	0.12	1.5×10^{-2}	5.6×10^{-3}
MFS	3.9×10^{-4}	3.4×10^{-5}	1.4×10^{-5}
Cracklet S	7.3×10^{-4}	5.9×10^{-5}	2.2×10^{-5}
Cracklet K	8.0×10^{-4}	5.7×10^{-5}	1.2×10^{-5}

Table 2
Errors in different norms for the methods considered for Simulation 1, now with the analytic g_b.

	$\|\|g_b - u_{120}\|\|_\infty$	$\|\|g_b - u_{120}\|\|_{\ell^2}$	$\|\|g_b - u_{120}\|\|_{\ell^1}$
BEM S	0.077	4.8×10^{-3}	1.1×10^{-3}
BEM K	0.12	1.5×10^{-2}	6.0×10^{-3}
MFS	3.7×10^{-5}	4.8×10^{-6}	2.0×10^{-6}
Cracklet S	9.9×10^{-5}	9.5×10^{-6}	3.3×10^{-6}
Cracklet K	1.6×10^{-5}	1.5×10^{-6}	4.0×10^{-7}

It should be noticed that the choice given by (41) is thought for convex shapes, because the edges of the cracklet may fall inside the domain, and θ_m must be considered small enough.

In Fig. 4 (left) we present the distribution of the cracklets, given 120 collocation points (20 each side), for $\delta_m = 5$, $\theta_m = 1$.

With these cracks we tested the Trefftz basis for cracklets K (double layer) and cracklets S (single layer), and compared the results with the results for the MFS, with the double number of collocation points, and using the same y_m as sources.

- **(a)** We considered the Dirichlet data given by the complex function ($z = x_1 + x_2 i$)

$$g_a(z) = \begin{cases} 0, & \text{if } Im(z) \le 0, \\ \frac{Im(z)}{10} Re\left(\frac{\sin(2z)}{1+i-z}\right) & \text{if } Im(z) > 0, \end{cases} \tag{42}$$

which is discontinuous in the derivatives, and presents a singularity at $1 + i$, meaning at the point (1,1) which is close to the boundary point $(\frac{3}{4}, 1)$.

In Fig. 4 (right), we plot the function in 1002 points on the boundary, starting with point (1,0) going anti-clockwise, and finishing on the same point.

In Fig. 5 (left) we plot the results using 120 cracklets S or K, or using 120 source points for the MFS. We may see that there is not much difference taking cracklets in the Trefftz method, or source points in the MFS, the results were similar in this case. The graph of the solution is given in Fig. 5 (right).

The highest values of the absolute errors occur in the corner points, especially in the corner point nearest to the singularity, as expected. Considering different norms, as in (29) and (30), we obtained the errors on the boundary (due to the maximum principle for Laplace equation the errors in the domain are smaller than the errors on the boundary), presented in Table 1.

It should be observed that the approximation given by the piecewise constant density in the BEM, either in the single layer formulation (BEM S), or in the double layer formulation (BEM K), is not good. For instance, with BEM K, the approximation with a piecewise discontinuous function performs poorly in the maximum norm, but is not so bad in the ℓ^2 or ℓ^1 norms. The ℓ^2 error for BEM K performed consistently like $O(h^{1.3})$, being h the average element length, and even with $N = 960$ elements ($h = 0.0071$), the ℓ^2 error was 1.9×10^{-3}.

On the other hand, by doing a simple dilation of the artificial boundary to $\gamma = 1.5\Gamma$, both indirect BEM, S or K, with $N = 120$, gave maximum errors about 10^{-3}, and ℓ^2 or ℓ^1 errors below 10^{-4}, being close to the errors obtained with the MFS or cracklets.

- **(b)** With exactly the same geometry, boundary points, cracklets, and point sources, we now considered the boundary function

$$g_b(z) = \frac{1}{10} Re\left(\frac{\sin(2z)}{1+i-z}\right), \tag{43}$$

which is almost the same function as considered in (42), but now it is only the real part of an analytic function on Ω and therefore it is the exact solution. Except for the BEM, the errors are comparatively smaller than before, due to the higher regularity, and the results are presented in a similar table (Table 2).

In Fig. 6 (left) we plot a similar figure to Fig. 5 (left), now with g_b as boundary function, and in Fig. 6 (right) we present the error in the whole domain, which is in average below 10^{-6}, except around the corner point, close to the singularity, where it is slightly higher.

Increasing the number of points near the corner singularity improves the results. For instance taking the same 120 points, but with a higher concentration at the corner, and at a distance $\delta_m = 10$, decreased the maximum absolute error of the MFS to 7×10^{-7} (50 times less than before), with a similar effect on the cracklet methods (4.2×10^{-6} for cracklets S and 1.4×10^{-6} for cracklets K).

4.2. Simulation 2 (mixed round shapes)

In this simulation we considered the same domain for $Im(z) > 0$ together with the semicircle $|z| < 1$, for $Im(z) < 0$. This defines Ω_2. The collocation points on the boundary $\partial\Omega_2$ and the cracklets are shown in Fig. 7 (left), at a similar distance $\delta_m = 5$. Again we used 20 points in each segment and 60 points on the semicircle, in a total of 120 collocation points, as before.

The results obtained for this shape and the data given by g_a or g_b are very similar to the previous case. In Fig. 7 (right) we present the variation of the absolute error for the three methods, considering the analytic boundary function g_b. The error results are presented in Table 3.

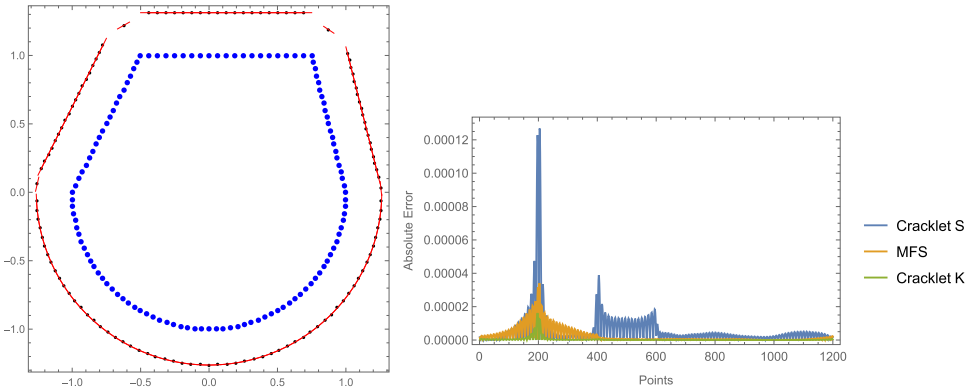

Fig. 7. Simulation 2. On the left, the collocation points (120 blue points) on the boundary $\partial\Omega_2$, and the cracklets (in red) using the procedure defined in (41). On the right, absolute error plots for the three methods, considering the boundary function g_b. (For interpretation of the references to color in this figure legend, the reader is referred to the web version of this article.)

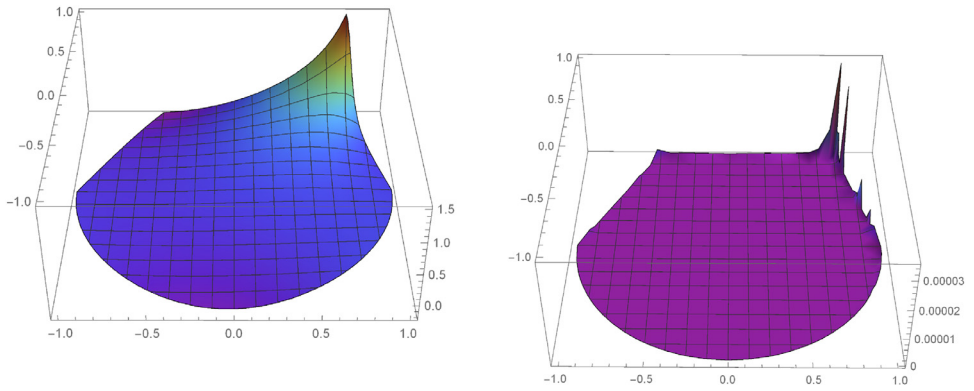

Fig. 8. Simulation 2. On the left, plot of the solution in the domain and, on the right, the error for the approximation obtained with 120 cracklets K.

Table 3
Errors in different norms for the 3 methods, considered for Simulation 2 with g_b.

	$\|\|g_b - u_{120}\|\|_\infty$	$\|\|g_b - u_{120}\|\|_{\ell^2}$	$\|\|g_b - u_{120}\|\|_{\ell^1}$
MFS	3.4×10^{-5}	4.8×10^{-6}	2.3×10^{-6}
Cracklet S	1.3×10^{-4}	1.3×10^{-5}	5.8×10^{-6}
Cracklet K	1.6×10^{-5}	1.4×10^{-6}	3.4×10^{-7}

Table 4
Errors in different norms for the 3 methods, considered for Simulation 3 with g_b.

	$\|\|g_b - u_{120}\|\|_\infty$	$\|\|g_b - u_{120}\|\|_{\ell^2}$	$\|\|g_b - u_{120}\|\|_{\ell^1}$
MFS	9.7×10^{-8}	4.0×10^{-8}	3.4×10^{-8}
Cracklet S	5.2×10^{-7}	9.0×10^{-8}	6.5×10^{-8}
Cracklet K	8.0×10^{-7}	8.9×10^{-8}	3.0×10^{-8}

In Fig. 8 we present the solution for the problem in Simulation 2 (on the left), and the absolute error for the approximation using cracklets K. As previously mentioned, for Simulation 1, the highest errors occur near the singularity, as expected.

4.3. Simulation 3 (round shapes)

We also considered shapes defined by parts of radial star-shape functions, in this case Ω_3 is defined by the boundary

$$\partial\Omega_3 = \left\{ r(t)e^{it} \ : \ t \in [0, 2\pi[\right\}, \quad \text{with } r(t) = \begin{cases} 1 - \frac{1}{3}\sin(3t) & t \in [0, \pi] \\ 1 & t \in]\pi, 2\pi[\end{cases} \tag{44}$$

The domain is presented in Fig. 9 (left) together with the associated cracklets, as defined in (41) at distance $\delta_m = 6$, and it presents two discontinuities (at $t = 0$, $t = \pi$).

As in the IBEM we could have used an artificial boundary to place the cracklets, but here we used the technique that is being considered for the MFS, in the distribution of source points (see [2]). Note that unlike the BEM, where the use of straight elements compromises the geometry of the boundary, here we may use collocation on the original boundary as long as these cracklets are placed outside the domain.

Using the boundary function g_b, in Fig. 9 (right) we present the variation of the absolute error for the three methods. The error results are presented in Table 4.

A similar table could be obtained for the function g_a, but with higher errors, nevertheless smaller than the ones obtained in Table 1.

Remark 4.1. It should be noted that in all these simulations we considered $\theta_m = 1$ in (41), but taking a different θ_m would slightly change the results. In this case, we also used $\theta_m = \frac{1}{4}, \frac{1}{2}, 2$, and the results were basically the same (only a slightly worse). This may be justified by the fact that, at a large distance from the boundary, the use of cracklet with half size is compensated by a coefficient taken as double the size.

4.4. Simulation 4 (non convex polygon)

In the previous cases the MFS provided good results, and now we will consider a case with discontinuous data, using a similar function to

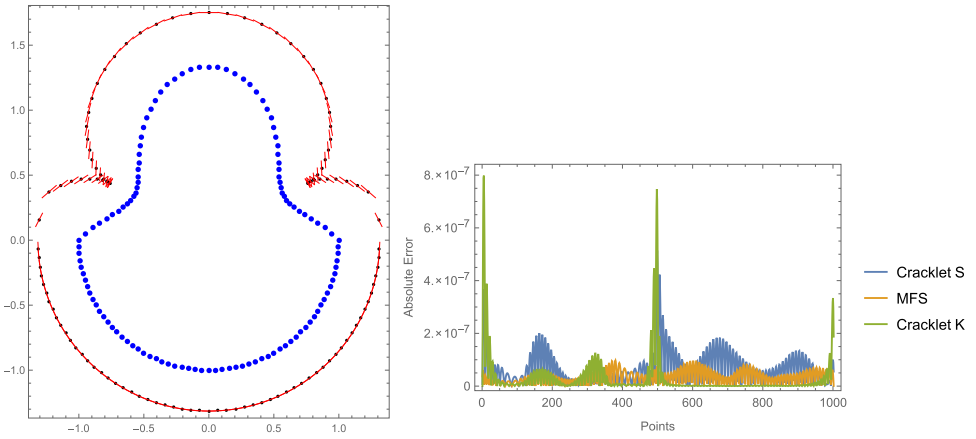

Fig. 9. Simulation 3. On the left, the collocation points (120 blue points) on the boundary $\partial\Omega_3$, and the cracklets (in red) using the procedure defined in (41). On the right, absolute error plots for the three methods, considering the boundary function g_b. (For interpretation of the references to color in this figure legend, the reader is referred to the web version of this article.)

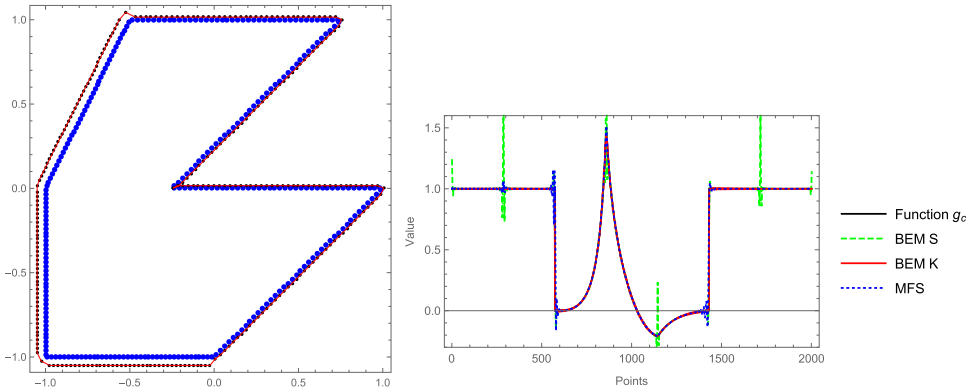

Fig. 10. Simulation 3. On the left, the collocation points (280 blue points) on the boundary $\partial\Omega_4$, and the used cracklets (in red). On the right, comparison of the plots for different methods, with $N = 280$ and the boundary function g_c. (For interpretation of the references to color in this figure legend, the reader is referred to the web version of this article.)

Table 5
Errors in different norms for the methods considered for Simulation 4, with the discontinuous function g_c.

	$\|\|g_c - u_{280}\|\|_{\ell^2}$	$\|\|g_c - u_{280}\|\|_{\ell^1}$
BEM S	7.7×10^{-2}	1.2×10^{-2}
BEM K	1.3×10^{-2}	2.8×10^{-3}
MFS	4.3×10^{-2}	7.1×10^{-3}
Cracklet S	3.0×10^{-2}	4.2×10^{-3}
Cracklet K	2.4×10^{-2}	2.5×10^{-3}

Table 6
Errors in different norms for the methods considered for Simulation 4, but now with the analytic function g_b.

	$\|\|g_b - u_{280}\|\|_{\infty}$	$\|\|g_b - u_{280}\|\|_{\ell^2}$	$\|\|g_b - u_{280}\|\|_{\ell^1}$
BEM S	0.22	7.9×10^{-3}	1.0×10^{-3}
BEM K	6.5×10^{-2}	5.6×10^{-3}	2.2×10^{-3}
MFS	2.0×10^{-3}	1.3×10^{-4}	4.7×10^{-5}
Cracklet S	8.0×10^{-3}	2.5×10^{-4}	3.0×10^{-5}
Cracklet K	1.1×10^{-2}	3.6×10^{-4}	2.5×10^{-5}

g_a but being 1 instead of 0, for $Im(z) \leq 0$. More precisely:

$$g_c(z) = \begin{cases} 1, & \text{if } Im(z) \leq 0, \\ g_a(z) & \text{if } Im(z) > 0, \end{cases} \tag{45}$$

Furthermore, we will consider a polygon with the same vertices as in Simulation 1, but with a new corner point $(-\frac{1}{4}, 0)$, with an angle greater than $\frac{3}{2}\pi$. We will call this domain Ω_4, which is represented in Fig. 10 (left) with the 280 collocation points on the boundary, together with cracklets placed on a surrounding curve with tip points y_m as given in (41), which is closer to the boundary for the first 4 segments, at a distance $\delta_m = 1$, and with $\delta_m = 5$, for the other 3 segments.

We also compared with the BEM S and BEM K (see the plots in Fig. 10, on the right), as the results were not so good in this case, and are given in Table 5.

We did not consider the maximum norm, as this is not appropriate for discontinuous functions, but we may see in Fig. 10 (right) that the BEM K was the most appropriate method in this case, since it is the one that best captures the discontinuities. On the other hand, BEM S, fitted the function, but presented high instabilities in the corner points. The MFS and the cracklet S or K methods also presented difficulties to fit the discontinuities, due to the Gibbs effect. In fact, since the cracklets were placed outside the boundary all functions are analytic there, and the Gibbs effect occurs.

We also considered the simulation for the same geometry, but now for the analytic function g_b, and as expected, the results are much better, especially for the Trefftz methods (MFS, cracklets S and K), as we may see in the error Table 6.

4.5. MFS enrichment

Finally we considered the possibility of combining methods to improve the results obtained in Table 5.

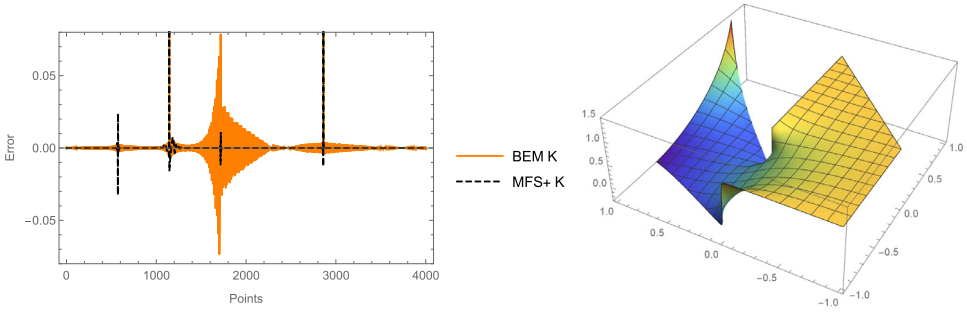

Fig. 11. Simulation 4. Comparison of the errors between MFS + K and BEM (on the left), and the solution for g_c given with the MFS + K (on the right).

Table 7
Improving the MFS with 7 edge cracklets K, for the discontinuous function g_c.

	$\|\|g_c - u_{280}\|\|_{\ell^2}$	$\|\|g_c - u_{280}\|\|_{\ell^1}$
BEM K	1.3×10^{-2}	2.8×10^{-3}
MFS	4.3×10^{-2}	7.1×10^{-3}
MFS + K	1.1×10^{-2}	4.7×10^{-4}

We took the MFS enriched by cracklets K.

This meant to consider 7 cracklets K, one at each edge of the polygon, to avoid the Gibbs effect on discontinuities and corner problems, and this also meant to place the cracks near the boundary, at a very close distance(= 10^{-4}).

To keep the same number of basis functions as before, we considered 273 source points for the MFS, using the 7 cracklets as an enrichment of the MFS and kept the distance $\delta_m = 1$ for all source points y_m as defined in (41).

The results of this method (abbreviated MFS + K) were much better than the ones of the MFS, and also better than BEM K, as we may see in Table 7 (we used 4008 test points on the boundary).

The biggest improvement was cancelling the Gibbs effect in the MFS, but difficulties remained in the corners. This lead to a considerable decrease in the average error, i.e. in the ℓ^1 norm, as the error at each point was below 10^{-3} except around 4 corner points, as we may see in Fig. 11 (left), compared to the worse performance of the BEM with double layer formulation using 280 elements, not affected by the corners, but with difficulties matching the peak of the boundary function g_c.

We present the solution given by this MFS + K method in Fig. 11 (right).

We could also consider more than 7 cracklets K, taking several more on each side, but this also generates further discontinuities at the end of each cracklet, as the functions $K(\gamma_n)$ are discontinuous at the tips. To avoid this we could also add $K_1(\gamma_n)$ cracklets as mentioned in Remark 3.2, but this goes beyond the scope of this paper, as this would also mean a comparison with BEM K formulated with piecewise linear, and not piecewise constant, densities.

5. Conclusions

In this work we presented two Trefftz methods with cracklets, based on the single layer potential (cracklet S) or the double layer potential (cracklet K), that in some particular situations may be viewed as a direct or as an indirect BEM, or may also be viewed as equivalent to the MFS with monopole or dipole source points. This depends if the cracklets are placed on the boundary (direct BEM), form a boundary outside (indirect BEM), or may be considered with small crack support (MFS). However, understanding these cracklets as the basis functions of a Trefftz method allows all these possibilities, and allows to establish a more flexible link between the methods.

For smooth boundary conditions the proposed Trefftz methods with cracklets perform in a similar way as the MFS and significantly better than the direct BEM. On the other hand, in the presence of discontinuities, the cracklets improve the accuracy of the MFS, if their supports are chosen on the boundary. In particular, we considered the cracklets as an enrichment of the MFS that proved to be helpful to avoid the Gibbs effect on discontinuous boundary conditions (as was already suggested in [5]).

The simulations have been carried for the Dirichlet problem of the Laplace equation in 2D, but may be extended with no great difficulty to Neumann or Robin boundary conditions, with the same performance of the method. It is also possible to consider other differential operators with a known fundamental solution, and an extension to 3D, but this would lead to new cracklet functions (some of which are already known from BEM research), and some extra difficulties with the 3D geometries are expected. This work is currently under investigation.

Acknowledgments

The financial support received from the Fundação para a Ciência e a Tecnologia (FCT) project UID/Multi/ 04621/2013 is gratefully acknowledged.

References

[1] Alves CJ, Abdallah JB, Jaoua M. Recovery of cracks using a point-source reciprocity gap function. Inverse Probl. Sci. Eng. 2004;12(5):519–34.
[2] Alves CJS. On the choice of source points in the method of fundamental solutions. Eng. Anal. Bound. Elem. 2009;33(12):1348–61.
[3] Alves CJS, Leitão VMA. Crack analysis using an enriched MFS domain decomposition technique. Eng. Anal. Bound. Elem. 2006;30(3):160–6.
[4] Alves CJS, Martins NFM. The direct method of fundamental solutions and the inverse kirsch- kress method for the reconstruction of elastic inclusions or cavities. J. Int. Equ. Appl. 2009;21(2):153–78.
[5] Alves CJS, Valtchev SS. On the application of the method of fundamental solutions to boundary value problems with jump discontinuities. Appl. Math. Comput. 2018;320:61–74.
[6] Antunes PRS, Valtchev SS. A meshfree numerical method for acoustic wave propagation problems in planar domains with corners and cracks. J. Comput. Appl. Math. 2010;234(9):2646–62.
[7] Barnett AH, Betcke T. Stability and convergence of the method of fundamental solutions for Helmholtz problems on analytic domains. J. Comput. Phys. 2008;227:7003–26.
[8] Chen CS, Karageorghis A, Li Y. On choosing the location of the sources in the MFS. Numer. Algor. 2015;72(1):107–30.
[9] Chen G, Zhou J. Boundary Element Methods with Applications to Nonlinear Problems. Atlantis Press; 2010.
[10] Chen J-T, Tsai J-J, Lee Y-T, Lee J-W. Study on connections of the MFS, trefftz method, indirect BIEM and invariant MFS in the three-dimensional laplace problems containing spherical boundaries. Appl. Math. Comput. 2011;218(8):4056–74.
[11] Chen W, Wang F. A method of fundamental solutions without fictitious boundary. Eng. Anal. Bound. Elem. 2010;34(5):530–2.
[12] Cheng AH-D, Cheng DT. Heritage and early history of the boundary element method. Eng. Anal. Bound. Elem. 2005;29(3):268–302.
[13] Fairweather G, Karageorghis A. The method of fundamental solutions for elliptic boundary value problems. Adv. Comput. Math. 1998;9(1/2):69–95.
[14] Golberg MA, Chen CS. The method of fundamental solutions for potential, Helmholtz and diffusion problems. In: Boundary Integral Methods: Numerical and Mathematical Aspects. WIT Press, Computational Mechanics Publications, Boston, Southampton; 1999. p. 103–76.
[15] Hon YC, Chen W. Boundary knot method for 2d and 3d helmholtz and convection-diffusion problems under complicated geometry. Int. J. Numer. Meth. Eng. 2003;56(13):1931–48.
[16] Jung J-H. A note on the Gibbs phenomenon with multiquadric radial basis functions. Appl. Numer. Math. 2007;57(2):213–29.

[17] Karageorghis A, Lesnic D, Marin L. A survey of applications of the MFS to inverse problems. Inverse Probl. Sci. Eng. 2011;19(3):309–36.
[18] Katsurada M, Okamoto H. A mathematical study for the charge simulation method I. J. Fac. Sci. Univ. Tokyo Sect. 1A Math. 1988;35:507–18.
[19] Kress R. Linear Integral Equations. Applied Mathematical Sciences, 82. 2nd. Springer; 1999.
[20] Li Z-C, Lu T-T, Huang H-T, Cheng AH-D. Trefftz, collocation, and other boundary methods—a comparison. Numer. Meth. Partial Differ. Equ. 2006;23(1):93–144.
[21] Šarler B. Solution of potential flow problems by the modified method of fundamental solutions: Formulations with the single layer and the double layer fundamental solutions. Eng. Anal. Bound. Elem. 2009;33(12):1374–82.
[22] Schaback R. An adaptive numerical solution of mfs systems. In: The Method of Fundamental Solutions - A Meshless Method. Dynamic Publishers; 2008. p. 1–27.
[23] Young D, Chen K, Lee C. Novel meshless method for solving the potential problems with arbitrary domain. J. Comput. Phys. 2005;209(1):290–321.
[24] Young DL, Huang YJ, Wu CS, Sladek V, Sladek J. Angular basis functions formulation for 2D potential flows with non-smooth boundaries. Engineering Analysis with Boundary Elements 2015;61:1–15.
[25] Li X, Oh J, Wang Y, Zhu H. The method of transformed angular basis function for solving the Laplace equation. Engineering Analysis with Boundary Elements 2018;93:72–82.